Optics Letters

Increasing applicability of slow light in molecular aggregate nanofilms with two-exciton dynamics

E. Díaz,[1,*] G. C. Martínez-Calzada,[1] E. Cabrera-Granado,[2] and O. G. Calderón[2]

[1]GISC, Departamento de Materiales, Universidad Complutense, E-28040 Madrid, Spain
[2]Departamento de Óptica, Universidad Complutense, E-28037 Madrid, Spain
*Corresponding author: elenadg@ucm.es

Received 25 March 2016; revised 23 April 2016; accepted 24 April 2016; posted 25 April 2016 (Doc. ID 260897); published 25 May 2016

We study the slow-light performance in the presence of exciton–exciton interaction in films of linear molecular aggregates at the nanometer scale. In particular, we consider a four-level model to describe the creation/annihilation of two-exciton states that are relevant for high-intensity fields. Numerical simulations show delays comparable to those obtained for longer propagation distances in other media. Two-exciton dynamics could lead to larger fractional delays, even in presence of disorder, in comparison to the two-level approximation. We conclude that slow-light performance is a robust phenomenon in these systems under the increasing complexity of the two-exciton dynamics.

OCIS codes: (190.4400) Nonlinear optics, materials; (190.5530) Pulse propagation and temporal solitons; (230.1150) All-optical devices.

http://dx.doi.org/10.1364/OL.41.002569

Slow-light research has shown a great potential in many different applications such as information technology, interferometry, or laser physics as a tool to enhance light-matter interactions. However, the overall effect on optical pulses is usually constrained by the necessity of long interacting media. There has been recent exciting research that provides compact slow-light devices and reduces the interacting length without limiting the obtained delay. Group velocities of $c/100$ have been achieved in 100 μm semiconductor waveguides at GHz frequencies [1]. More recently, Kim *et al.* [2] proposed composites doped with metal nanoparticles to obtain fractional delays (ratio between delay and temporal width of the input pulse) of 2 for 5 μm propagation lengths, or even ∼40 for 90 μm using a noncollinear pumping scheme. Slow light has also been employed to enhance the gain in active semiconductor waveguides [3] which may be used in ultra-compact amplifiers and optical modulators of ∼100 μm [4] due to the increase in modulation efficiency.

Reducing the slow-light devices to the nanometer scale has been proposed by using coherent population oscillations (CPO) in J-aggregate nanofilms [5]. J-aggregates are molecular assemblies that show coherently coupled transition dipole moments and an absorption band that is narrower and redshifted with respect to the monomer band [6]. They have shown great possibilities in photonic applications, thanks to their enhanced nonlinear response and narrow absorption line. This leads, for example, to a coherent coupling of excitons with cavity modes or plasmons in metallic nanostructures [7]. In a previous work, fractional delays up to ∼0.5 were shown with constrained distortion for input pulses of roughly a 10 GHz bandwidth in ultrathin films of some tens of nanometers [5]. This work analyzed CPO-based slow light in J-aggregates for optical pulses resonant with the transition to the one-exciton band, while creation and annihilation of two excitons were not considered. Gain of the probe pulse was also shown, in contrast to the residual absorption observed in other slow-light media such as optical fibers. Moreover, disorder effects typically present in these systems, although reducing the attainable delay, have a relatively low impact on slow-light performance.

One-to-two exciton transitions in J-aggregates were first observed by Fidder *et al.* [8] in a pump-probe experiment on pseudo-isocyanine-bromide (PIC-Br). Glaeske *et al.* [9] showed that such a transition and exciton annihilation play a crucial role in the conditions for achieving optical bistability. Multiexciton states have also been exploited to coherently control the electromagnetic field inside a cavity [10] and are essential in strong coupling with plasmonic structures [11].

In this Letter, we address how the two-exciton dynamics influence slow-light performance of linear J-aggregates nanofilms. Films are considered to be formed by an ensemble of linear molecules oriented parallel to each other and to the film surface. Despite being formed by thousands of molecules, only coherent segments with length N are relevant for optical applications due to the state localization in presence of disorder. We model disordered molecular aggregates as an ensemble of homogeneously broadened four-level systems of coherence length N. See [9] for a detailed description of the model. Particularly, we simulate three excitonic levels with $|0\rangle$, $|1\rangle$, and $|2\rangle$ excitons. After the creation of the state $|2\rangle$, exciton–exciton annihilation takes place by resonant interaction with a high molecular electronic-vibrational level $(3)_{e-vib}$. Then, a fast phonon-assisted relaxation is produced to the ground vibrational state, to finally de-excite to $|0\rangle$ or $|1\rangle$ excitonic states. Figure 1 represents the schematics of the model and the pulse propagation through the nanofilm.

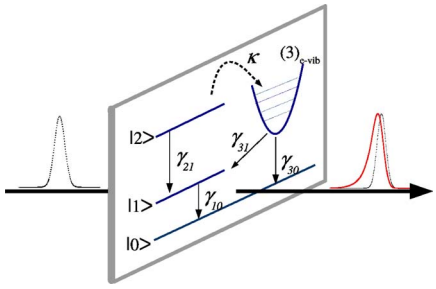

Fig. 1. Schematic view of the aggregate nanofilm modeled as an ensemble of four-level systems. Input signal (dashed line) propagating from left to right through the nanofilm results in a delayed output signal (solid line). Pulses are shown according to numerical simulations.

Bloch equations under rotating wave and slowly varying amplitude approximations for this system read

$$\begin{aligned}
\dot{\rho}_{00}^N &= id_{10}^N(\sigma_{10}^N E^* - \sigma_{10}^{N*}E)/4\hbar + \gamma_{10}^N\rho_{11}^N + \gamma_{30}^N\rho_{33}^N,\\
\dot{\rho}_{11}^N &= id_{21}^N(\sigma_{21}^N E^* - \sigma_{21}^{N*}E)/4\hbar - id_{10}^N(\sigma_{10}^N E^* - \sigma_{10}^{N*}E)/4\hbar\\
&\quad - \gamma_{10}^N\rho_{11}^N + \gamma_{21}^N\rho_{22}^N + \gamma_{31}^N\rho_{33}^N,\\
\dot{\rho}_{22}^N &= -id_{21}^N(\sigma_{21}^N E^* - \sigma_{21}^{N*}E)/4\hbar - (\gamma_{21}^N + \kappa)\rho_{22}^N,\\
\dot{\rho}_{33}^N &= -(\gamma_{30}^N + \gamma_{31}^N)\rho_{33}^N + \kappa\rho_{22}^N,\\
\dot{\sigma}_{10}^N &= [i(\omega - \omega_{10}^N) - \Gamma_{10}^N]\sigma_{10}^N\\
&\quad - id_{10}^N(\rho_{11}^N - \rho_{00}^N)E/\hbar + id_{21}^N\sigma_{20}^N E^*/2\hbar,\\
\dot{\sigma}_{21}^N &= [i(\omega - \omega_{21}^N) - \Gamma_{21}^N - \kappa/2]\sigma_{21}^N\\
&\quad - id_{21}^N(\rho_{22}^N - \rho_{11}^N)E/\hbar - id_{10}^N\sigma_{20}^N E^*/2\hbar,\\
\dot{\sigma}_{20}^N &= [i(\omega - \omega_{10}^N) + i(\omega - \omega_{21}^N) - \Gamma_{20}^N - \kappa/2]\sigma_{20}^N\\
&\quad + id_{21}^N\sigma_{10}^N E/2\hbar - id_{10}^N\sigma_{21}^N E/2\hbar. \qquad (1)
\end{aligned}$$

Here, ω and E are the frequency and slowly varying amplitude of the field, respectively. The population of the energy level j is denoted by ρ_{jj}^N, while σ_{ij}^N are the slowly varying amplitudes of the off-diagonal density matrix elements. The latter accounts for the coherences between the energy levels (i, j). The transition frequency and the dipole moment within those levels of every segment read ω_{ij}^N and $d_{ij}^N = d_{ij}^1\sqrt{N}$, respectively. Here, the superscript 1 refers to single-molecule properties. The relaxation rate due to spontaneous emission is $\gamma_{ij}^N = N\gamma_{ij}^1$, while Γ_{ij}^N is the decay of the coherence σ_{ij}^N. Furthermore, $\Gamma_{10}^N = \gamma_{10}^N/2 + \Gamma$, $\Gamma_{21}^N = \gamma_{10}^N/2 + \gamma_{21}^N/2 + \Gamma$, and $\Gamma_{20}^N = \gamma_{21}^N/2 + \Gamma$, where Γ accounts for pure dephasing processes. The vibronic state $(3)_{e\text{-}vib}$ relaxes to states $|0\rangle$ and $|1\rangle$ with rates γ_{30}^N and γ_{31}^N, respectively. Last, κ refers to the exciton–exciton annihilation constant.

Size dispersion of the coherent segments translates into an inhomogeneous broadening affecting the J-band at low temperatures, which mainly gives rise to the fluctuation of the transition energies $\hbar\omega_{10}^N$ [12]. Thus, we will substitute all size-dependent quantities, except ω_{10}, by their mean values in the aggregate, and we will remove the index N hereafter. For brevity, we will refer to the field by way of the Rabi frequency defined in units of Γ_{10} as $\Omega = dE/\hbar\Gamma_{10}$ from now on, where $d = \sqrt{(d_{10}^2 + d_{21}^2)/2}$.

We will first study the response of the system to a sinusoidally modulated signal $\Omega = \Omega_0 + \Omega_m \sin(\delta t)$. Assuming normal propagation and parallel polarization of the incident field to the transition dipole moments of all the aggregates and to the film plane, the equation for the field inside the film reads

$$\Omega = \Omega^{\text{in}} + i\gamma_R\sum_N p(N)(\mu_{10}\sigma_{10} + \mu_{21}\sigma_{21}). \qquad (2)$$

Here, the last term is the electric polarization of the disordered molecular aggregates, where $\mu_{10} = d_{10}/d$, $\mu_{21} = d_{21}/d$, and $p(N)$ refer to the disorder distribution over localization lengths. The parameter $\gamma_R = \mu_0|d|^2N_0c\omega L/2\hbar\Gamma_{10}$ describes the collective superradiant damping of an ensemble of four-level molecules, N_0 being the density of localization segments. The transmittance T and the dephasing ϕ induced by the film are calculated by the ratio between the output and input signals: $\frac{\Omega_m}{\Omega_m^{\text{in}}} = T\exp^{i\phi}$. Thus, the fractional delay is defined as $F = \phi/2\pi$.

Let us start analyzing the case of no size dispersion. For simplicity, hereafter we consider an incident field resonant with the lower energy transition of the system, $\omega = \omega_{10}$. We take the parameters of PIC-Br as it is one of the most studied J-aggregates. The magnitude of the nearest-neighbor coupling has been established as $J = 0.08$ eV, which gives rise to the transition energy shift $\omega_{21} - \omega_{10} = 3\pi^2J/N^2\hbar = 0.25$ THz. We use $\gamma_{10} = 1/37$ ps^{-1} (corresponding to a homogeneous aggregate of size $N = 100$), $\Gamma_{10} = \gamma_{10}/0.02$, and $\kappa = 5$ ps^{-1}. These values are consistent with measurements at low temperatures [13,14] and allow direct comparison with previous CPO works [15]. The transition dipole moment between $|0\rangle$ and $|1\rangle$ is $d_{10}^1 = 12.1$ D, and the concentration of aggregates is $N_0 \sim 10^{23}$ m^{-3}. The dipole moment and the spontaneous emission of the transition between $|1\rangle$ and $|2\rangle$ are taken as $d_{21} = \sqrt{1.5}d_{10}$ and $\gamma_{21} = 1.5\gamma_{10}$. Here, we have considered the average ratio of the oscillator strength of the relevant transitions as $f_{21}/f_{10} \sim d_{21}^2/d_{10}^2 \sim 1.5$ [14]. Last, though to the best of our knowledge, there is no experimental measurement of the rates γ_{31} and γ_{30}, the employed values in this Letter are based on those found in the bibliography on exciton–exciton annihilation in J-aggregates [16]. For simplicity, we take equal decay values $\gamma_{30} = \gamma_{31} = \gamma_v\gamma_{10}$. According to our simulations, relevant figures of merit for slow-light performance arise if $(\gamma_{30} + \gamma_{31}) \gtrsim \gamma_{10}$, so this will be the case in the following numerical study.

Figure 2 depicts the fractional delay and transmittance, calculated by the integration of Eq. (1) as a function of the modulation frequency δ and different values of γ_v. In this figure and, hereafter, we only show results for the saturation intensity and $\gamma_R \lesssim \gamma_R^*$, where CPO-based slow light attains maximum delay [5]. If $\gamma_R < \gamma_R^*$, the fractional delay is reduced while, for $\gamma_R > \gamma_R^*$, the system shows bistability, which introduces a large distortion of the output signal. Notice that γ_R^* depends on γ_v. Figure 2(a) shows that the particular values of γ_v have no significant effect on the achieved maximum fractional delay ($F \sim 0.2$). However, an increasing value of γ_v shifts the optimum frequency to higher values, up to ~35 GHz for $\gamma_v = 3$. Figure 2(b) shows an increasing transmission with a larger γ_v as well. As was already shown for the one-exciton approximation [5], there is gain in the weak sinusoidal modulation due to energy transfer between the background field and the sideband. This effect represents a remarkable advantage in

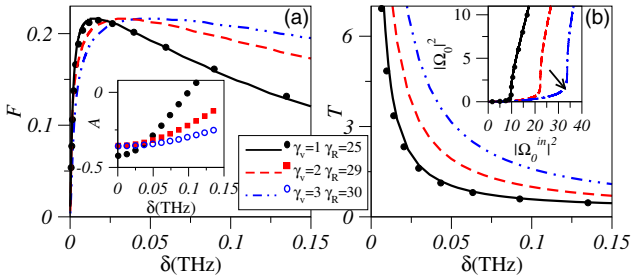

Fig. 2. (a) Fractional delay and (b) transmittance of a sinusoidal input signal as a function of the modulation frequency δ for different values of the ratio γ_v in absence of disorder. Inset (a) shows the absorption hole of the weak field. Inset (b) presents the output–input curve for the strong field $|\Omega_0|^2$, with the arrow pointing the saturation intensity for $\gamma_v = 3$. The symbols result from analytical calculations based on Eq. (3).

contrast with the undesired residual absorption present in other CPO-based slow-light devices.

We now focus on the system response under illumination with a Gaussian-like pulse $\Omega = \Omega_0 + \Omega_m \exp\left(\frac{-2\sqrt{\mathrm{Log}(2)}t}{\mathrm{FWHM}}\right)^2$. Here, FWHM refers to the full width at half-maximum of the temporal pulse. In this case, not only the attainable delay, but also the distortion of the output pulses is relevant for applications. We define distortion D as the ratio between the output and input pulse standard deviations. Figure 3 shows the fractional delay and distortion as a function of the input pulse temporal width. It can be seen that the pulse with maximum delay exhibits a large distortion. However, imposing a limit of $D = 2$ (standard in slow-light experiments), values up to $F = 0.4$–0.5 are obtained for 70 ps long pulses, which gives rise to a ∼14 GHz bandwidth. As mentioned before, increasing values of γ_v blueshift the maximum delay and reduce the optimal pulse width. Lower distortions can be obtained by reducing the incident intensity below the optimal one. This also reduces the delay, although it remains in a relevant order of magnitude for slow-light performance, as shown in Fig. 3 with symbols. The inset of Fig. 3 shows how the signal transmittance is mostly larger than 1, in agreement with Fig. 2. These results show that two-exciton dynamics lead to larger fractional delays for similar values of distortion in comparison to the two-level approximation.

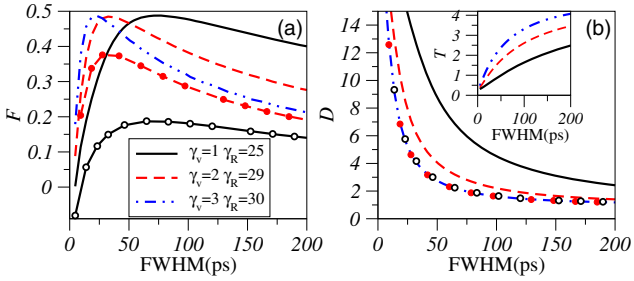

Fig. 3. (a) Fractional delay, (b) distortion and (inset) transmittance for pulsed input signals against the initial pulse temporal width (FWHM) in absence of disorder. Different values of γ_v are considered. Lines with empty dots ($\gamma_v = 1$) and solid dots ($\gamma_v = 2$) show delays for incident intensities below the saturation point which reproduce the constrained distortion obtained for $\gamma_v = 3$.

To gain insight into the previous results, we turn to a more tractable model by assuming the following approximations in Eq. (1). We neglect atomic coherence effects by eliminating σ_{20} for $\dot{\sigma}_{10}$ and $\dot{\sigma}_{21}$. We also neglect the population $\rho_{22} \simeq 0$ since the exciton–exciton annihilation time is much faster than the rest of the decay times. Then, we adiabatically eliminate the coherences σ_{10} and σ_{21}, as usual in CPO studies, since dephasing times are much shorter than the population decay times. Last, we also consider that the frequency of the incident field nearly matches the frequencies of the two relevant transitions. In the following, we will show that the resulting system retains the fundamental features of the full four-level model of Eq. (1). This simplified model reads

$$\begin{aligned}
\dot{\rho}_{11} &= -\gamma_{10}\rho_{11} + \gamma_{31}\rho_{33} - \frac{\mu_{21}^2\Gamma_{10}^2\Omega^2}{2\Gamma_{21}+\kappa}\rho_{11} \\
&\quad - \frac{\mu_{10}^2\Gamma_{10}\Omega^2(2\rho_{11}+\rho_{33}-1)}{2}, \\
\dot{\rho}_{33} &= -(\gamma_{30}+\gamma_{31})\rho_{33} + \frac{\mu_{21}^2\Gamma_{10}^2\Omega^2}{2\Gamma_{21}+\kappa}\rho_{11}, \\
\frac{\Omega^{\mathrm{in}}}{\Omega} &= 1 - \gamma_R\left(\mu_{10}^2(2\rho_{11}+\rho_{33}-1) - \frac{2\mu_{21}^2\Gamma_{10}}{2\Gamma_{21}+\kappa}\rho_{11}\right). \qquad \textbf{(3)}
\end{aligned}$$

Similar to what was studied in Fig. 2, we consider a sinusoidally modulated incident field $\Omega = \Omega_0 + \Omega_m \exp(-i\delta t) + \mathrm{c.c.}$ that induces a periodic modulation of the populations at the beat frequency δ, i.e., $\rho_{jj} = \rho_{jj}^0 + \rho_{jj}^m \exp(-i\delta t) + \mathrm{c.c.}$. The coherent population oscillation modifies the absorption of the sidebands which leads to slow-/fast-light propagation. We insert this expansion in Eq. (3) and equate terms oscillating at the same harmonic of δ. The 0-order term gives us the behavior of the strong field Ω_0; see the inset of Fig. 2(b). The first-order term in δ gives us the amplitude of the population oscillation and the sidebands fields. Then, we compute the transmission and delay time suffered by the sideband. Figures 2(a) and 2(b) show a good agreement between the full integration of Eq. (1) and the analytical results given by this simplified model. The imaginary part of the susceptibility χ at the modulation frequency δ can also be easily obtained from Eq. (3). The inset of Fig. 2(a) depicts the characteristic hole in absorption present in CPO processes $A = \mathrm{Im}(\chi_m)/\mathrm{Im}(\chi_0)$. It can be seen how it broadens as γ_v increases, which explains the blueshift found in the maximum delay (see Figs. 2 and 3). To finish the study of the ordered system, we study the maximum fractional delay F_{opt} (versus δ) by increasing the parameter γ_v and the input Rabi frequency; see Fig. 4(a). Figure 4(b) shows F_{opt} as a function of the input intensity for $\gamma_v = 3$. Two local maxima of F_{opt} can be seen for each value of γ_v. The first at lower input intensities relates to creation of one exciton while the second arises at higher intensities which allow generation/annihilation of two excitons in the aggregate. The characteristic times of population dynamics in these maxima are $\delta_{\mathrm{opt}} \sim \gamma_{10}$ and $\delta_{\mathrm{opt}} \sim \gamma_{30} + \gamma_{31}$, respectively. The latter could take higher values than γ_{10}, giving rise to a larger bandwidth with lower distortion; see Fig. 3. Moreover, by analyzing Eq. (3), it can be demonstrated that such an optimal functionality could be achieved for $\gamma_R \lesssim 33$. This collective parameter can be obtained by modifying the temperature or increasing the aggregate concentration within reasonable experimental conditions.

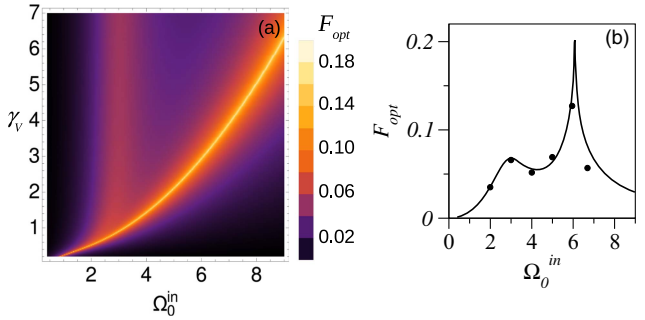

Fig. 4. (a) Maximum fractional delay obtained from Eq. (3) as a function of the ratio γ_v and the input strong field Ω_0^{in}. (b) Right plot represents a comparison between the simplified model (solid line) and the full integration of Eq. (1) (dots) for $\gamma_v = 3$.

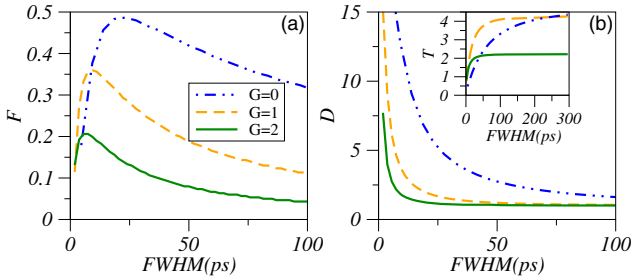

Fig. 5. (a) Fractional delay, (b) distortion and (inset) transmittance for pulsed input signals against FWHM for the ratio $\gamma_v = 3$. Different magnitudes of disorder G are considered.

Last, we analyze the effects of size dispersion on the slow-light performance for input pulsed signals. Aggregates are formed by coherent segments of different length N, such that disorder effects can be modeled by a discrete distribution $p(N)$ with mean $\bar{N}$ and standard deviation a. In [12], it was demonstrated that $p(N)$ can be replaced by a continuous one of transition energies ω_{10}^N. Thus, such N-dependency is introduced into the detunings Δ_{10}^N and, Δ_{21}^N while it is neglected for the rest of parameters. In this Letter, we integrate Eq. (1) for every coherent segment to calculate its contribution to the electric polarization in Eq. (2). Finally, to obtain the total molecular field, we average such terms with the following Gaussian distribution:

$$\sum_N p(N) = \sum_N \frac{\exp\left(\frac{-(N-\bar{N})^2}{2a^2}\right)}{\sqrt{2\pi a^2}} \to \int_{-\infty}^{\infty} \frac{\exp\left(\frac{-(\Delta_{10}^N-\Delta_{10})^2}{2\,G^2}\right)}{\sqrt{2\pi G^2}} \mathrm{d}\Delta_{10}^N. \tag{4}$$

Here, $G = 2\pi^2 Ja/\hbar\Gamma_{10}\bar{N}^3$ denotes the magnitude of the J-bandwidth resulting from the inhomogeneous broadening and Δ_{10} refers to the detuning respect to the central frequency of the Gaussian. Similarly to the two-level approximation, the maximum attainable delays are reduced when G increases. However, we show that this nondesirable effect is much more constrained in the current four-level model; see Fig. 5(a). For example, a magnitude of disorder $G = 2$ reduces the fractional delay up to 2.5 times with respect to the value obtained without size dispersion. However, this reduction is lower than that found in the two-level approximation where delays resulted 4 times lower [5]. Moreover, similarly to what was shown in that work, the detrimental effect of a larger inhomogeneous linewidth can be compensated by increasing the value of γ_R. More importantly, as a new feature of the current model, the presence of disorder results in a remarkable blueshift of the pulse bandwidth susceptible of slow-light performance up to values close to 100 GHz. In such a case the delay is still relevant for applications, $F \simeq 0.2$ for $G = 2$, while keeping $D \leqq 2$.

Finally, we look at the aggregate photostability under the considered illumination conditions. For example, taking the optimum Rabi frequency inside the film $\Omega_0 \sim 1.7\Gamma_{10}$ for $\gamma_R = 30$ and a pulse width of 70 ps, we obtain an intensity of 1.3×10^{14} photons/cm^2 per pulse in the sample. This value is clearly below the damage threshold in experiments [17] ($\sim 10^{16}$ photons/cm^2 per pulse), so photobleaching is not expected to occur in the proposed optical device.

In summary, we have analyzed CPO-based slow light in a J-aggregate nanofilm under pulse intensities high enough to excite two-exciton dynamics. Fractional delays up to ~0.5 with constrained distortion can be obtained for pulse bandwidths of ~14 GHz. Size dispersion significantly increases this available bandwidth, up to values close to 100 GHz, maintaining a fractional delay close to 0.2. These figures of merit support J-aggregates as a promising candidate for slow-light devices at the nanoscale.

Funding. MINECO (MAT2013-46308, FIS2013-41709-P).

REFERENCES

1. J. Mørk, R. Kjær, M. van der Poel, and K. Yvind, Opt. Express **13**, 8136 (2005).
2. K.-H. Kim, A. Husakou, and J. Herrmann, Opt. Express **20**, 25790 (2012).
3. S. Ek, P. Lunnemann, Y. Chen, E. Semenova, K. Yvind, and J. Mork, Nat. Commun. **5**, 5039 (2014).
4. T. Baba, H. C. Nguyen, N. Yazawa, Y. Terada, S. Hashimoto, and T. Watanabe, Sci. Technol. Adv. Mater. **15**, 024602 (2014).
5. E. Cabrera-Granado, E. Díaz, and O. G. Calderón, Phys. Rev. Lett. **107**, 013901 (2011).
6. J. Knoester, Int. J. Photoenergy **2006**, 61364 (2006).
7. S. K. Saikin, A. Eisfeld, S. Valleau, and A. Aspuru-Guzik, Nanophotonics **2**, 21 (2013).
8. H. Fidder, J. Knoester, and D. A. Wiersma, J. Chem. Phys. **98**, 6564 (1993).
9. H. Glaeske, V. A. Malyshev, and K.-H. Feller, Phys. Rev. A **65**, 033821 (2002).
10. F. Herrera, B. Peropadre, L. A. Pachon, S. K. Saikin, and A. Aspuru-Guzik, J. Phys. Chem. Lett. **5**, 3708 (2014).
11. G. Zengin, M. Wersäll, S. Nilsson, T. J. Antosiewicz, M. Käll, and T. Shegai, Phys. Rev. Lett. **114**, 157401 (2015).
12. E. C. Jarque and V. A. Malyshev, J. Chem. Phys. **115**, 4275 (2001).
13. H. Fidder, J. Knoester, and D. A. Wiersma, Chem. Phys. Lett. **171**, 529 (1990).
14. K. Minoshima, M. Taiji, K. Misawa, and T. Kobayashi, Chem. Phys. Lett. **218**, 67 (1994).
15. R. W. Boyd, M. G. Raymer, P. Narum, and D. J. Harter, Phys. Rev. A **24**, 411 (1981).
16. H. Stiel, S. Daehne, and K. Teuchner, J. Lumin. **39**, 351 (1988).
17. R. V. Markov, Z. M. Ivanova, A. I. Plekhanov, N. A. Orlova, and V. V. Shelkovnikov, Quantum Electron. **31**, 1063 (2001).